J Mater Sci: Mater Electron (2022) 33:6059–6069

The electrical and dielectric characterization of the Co/ZnO-Rods/*p*-Si heterostructure depending on the frequency

Sakir Aydogan[1,2], Adem Kocyigit[3,*], Burcu Bozkurt Cirak[4], Erman Erdogan[3], and Mehmet Yilmaz[1,5,*]

[1] *Advanced Materials Research Laboratory, Department of Nanoscience and Nanoengineering, Graduate School of Natural and Applied Sciences, Ataturk University, 25240 Erzurum, Turkey*
[2] *Department of Physics, Science Faculty, Atatürk University, 25240 Erzurum, Turkey*
[3] *Department of Electronics and Automation, Vocational High School, Bilecik Seyh Edebali University, 11230 Bilecik, Turkey*
[4] *Department of Alternative Energy Sources, Vocational High School, Erzincan Binali Yıldırım University, 24000 Erzincan, Turkey*
[5] *Department of Science Teaching, K.K. Education Faculty, Ataturk University, 25240 Erzurum, Turkey*

Received: 15 November 2021
Accepted: 13 January 2022
Published online: 25 January 2022

ABSTRACT

Zinc oxide (ZnO) rods film was fabricated by homemade and simple spray pyrolysis technique on a *p*-type silicon (Si) substrate, and the film layer was employed as an interfacial material between the Co and *p*-type Si for obtaining Co/ZnO-Rods/*p*-Si heterostructure. The scanning electron microscopy (SEM) was used to discover the rods-like structures and uniform morphology of the ZnO film. The impedance spectroscopy technique was performed on the Co/ZnO-Rods/*p*-Si heterostructure to determine electrical and dielectric properties depending on the frequency. The *C*–*V* and *G*–*V* characteristics revealed that the electrical properties related to the frequency and voltage changes. The dielectric properties were studied depending on frequency by extracting dielectric constant (ε'), dielectric loss (ε''), loss tangent (tan δ), ac electrical conductivity (σ), and real and imaginary parts of the electric modulus (M' and M''). The results highlighted that the Co/ZnO-Rods/*p*-Si heterostructures can be employed for intermediate frequency applications.

1 Introduction

Metal oxides are very interesting and attractive materials due to their adjustable band gap and electrical behaviors with various synthesizing techniques and dopants [1–3]. Among the metal oxides, ZnO is a well-known and most studied metal oxide and, it has a suitable band gap as 3.37 eV for optoelectronic applications and a high dielectric constant of 8.5 [4, 5]. Enough high dielectric constant makes it good interlayer material for metal-semiconductor devices

Address correspondence to E-mail: adem.kocyigit@bilecik.edu.tr; yilmazmehmet32@gmail.com

https://doi.org/10.1007/s10854-022-07784-y

to stop unwanted electrical discharging as well as to provide well-capacitive behaviors [6].

Metal-semiconductor devices have been studied by various scientist because of their high importance in electronic and optoelectronic applications such as rectifying the current, switching the conductivity, and detecting the light [7–10]. The interface of the metal-semiconductor devices is important to control electrical behaviors between the metal and semiconductor because traps, unwanted disorders in the crystalline structures, and interface states can cause problems [11, 12]. To decrease these problems, proper materials such as metal oxides, insulators, or polymers are inserted between the semiconductor and metal in a good order [13–15]. For that reason, various metal oxides, as well as insulator layers, have been investigated as interfacial layers to manage the electrical conductivity of metal-semiconductor junctions [16, 17].

Polarization and conduction mechanism for metal-semiconductor devices are important to understand the electrical and dielectric properties [18, 19]. The polarization mechanism can be electronic, ionic, surface, or dipolar; polarization changes by the magnitude of the applied frequency [19]. The intermediate frequencies (10^3–10^6 Hz) are important for metal-semiconductor devices to reveal the frequency-dependent characteristics, and a non-dipole polarization is obtained related to the relaxation time (τ) due to existing impurities, surface charges, as well as orientable dipoles at that frequencies. [20]. Thus, the investigation of the polarization mechanism can provide to disclose the dielectric properties of the metal-semiconductor devices in the intermediate frequencies [21].

There are some studies in the literature to characterize the electrical and dielectric behaviors of the ZnO-based devices. Samuel et al. [22] synthesized ZnO nanorods by hydrothermal method, and they studied dielectric properties of the ZnO nanorods by impedance spectroscopy technique. The results revealed that the ZnO nanorods exhibited high dielectric constant at lower frequencies. Saravan et al.[23] investigated electrical and dielectric behaviors of the ZnO nanorods with substitution of various transition metals obtained by thermal decomposition process. They used impedance spectroscopy technique to characterize ZnO nanorods for wide range frequency and concluded that substitution elements affected the conductivity, dielectric loss, and relaxation time. Buyukbas-Ulusan et al. [24] studied electrical and dielectric properties of the various Cd-doped Al/Cd-doped ZnO/*p*-Si structures by *C*–*V* and *G*–*V* characteristics. They concluded that Cd doping increased the dielectric constant and decreased dielectric loss.

In this study, we obtained ZnO-rods thin film by easy and homemade spray pyrolysis technique and used the film in the interface of the Co/*p*-Si heterostructure to control electrical properties as well as provide passivate unwanted dangling bonds. The impedance spectroscopy technique was employed to determine electrical and dielectric characterization of the Co/ZnO-Rods/*p*-Si heterostructure for a wide range of frequencies. According to our best knowledge, there is no study on the Co/ZnO-Rods/*p*-Si heterostructure for dielectric characterization by spray pyrolysis technique.

2 Experimental details

Zinc chloride ($ZnCl_2$) was bought from Sigma-Aldrich Company and solved in distilled water to obtain 0.5 M solution by stirring 2 h on a magnetic stirrer by keeping the solvent temperature at 60 °C throughout the stirring process. A couple of HCl drops was added to the solution. Meanwhile, a *p*-type silicon with 5–10 Ω cm resistivity, 600 μm thickness, and (111) crystal plane orientation was used as a semiconductor material and divided into 2 cm^2 area pieces. Then, an ultrasonic cleaner was used to clean the sliced wafers in acetone, distilled water, and propanol solvents for 10 min of each solvent. HF:H_2O (ratio of 1:1 volume) mix solution was used to remove impurities and native oxide layer from the surfaces by dumping into the mix solution for 30 s. The wafer pieces were transferred into DC magnetron sputtering system to obtain 100 nm aluminum (Al) ohmic contact on the back of the substrates. The N_2 gas-filled oven was employed to anneal pieces for 3 min at 500 °C temperature. The ZnO solution was sprayed onto the *p*-Si substrates by a homemade spray pyrolysis system at 500 °C substrate temperatures. The substrate-nozzle distance and angle were kept at 40 cm and 45°, respectively. The Co metal was sputtered onto the ZnO layers as 150 nm thicknesses by DC magnetron sputtering system to obtain rectifying contact via 3.14×10^{-2} cm^2 squared hole array

mask. Figure 1 shows the schematic and band diagrams of the Co/ZnO-Rods/*p*-Si heterostructures.

The morphology of the ZnO surface was analyzed by FEI/Quanta 450 FEG SEM. The Co/ZnO-Rods/*p*-Si heterostructures were characterized by HP 4192A LF Impedance Analyzer System to obtain *C*–*V* as well as *G*–*V* characteristics.

3 Results and discussion

Figure 2 reveals the SEM image of the fabricated ZnO films by spray pyrolysis technique. The ZnO film surfaces exhibit homogenously distributed rods and smooth surfaces, and there are no cracks and pinholes. The morphology of the fabricated ZnO layer on the silicon substrate highlights the proper interfacial layer behavior for metal-semiconductor devices. The rod radii change between 100 and 800 nm according to the SEM image in Fig. 2. This kind of rod behavior can be found in the literature for the ZnO layer obtained by spray pyrolysis technique [25, 26].

C–*V* plots of the Co/ZnO-Rods/*p*-Si heterostructure are displayed in Fig. 3 depending on the changing frequency from 10 kHz to 1 MHz. The capacitance profile exhibited peaks for the frequency range of 10 kHz and 700 kHz owing to having the defects that were formed during the film producing process or interface states in the heterostructure [27]. The peaks region shifted to forward bias, and their intensity decreased with increasing frequency due to that alternative current (ac) signal could not be followed by interface states [21]. Normally, the peak position is seen in the accumulation region for the

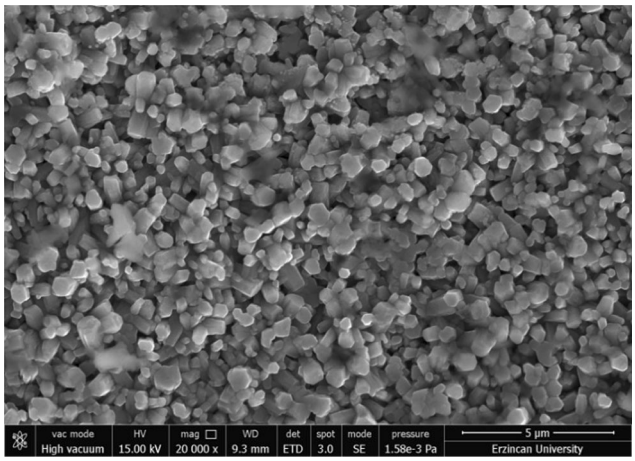

Fig. 2 SEM image of the ZnO-Rods interlayer films

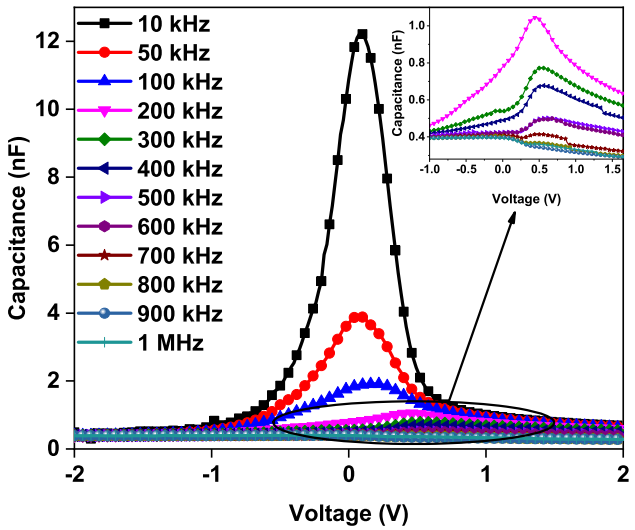

Fig. 3 *C*–*V* characteristics of the Co/ZnO-Rods/*p*-Si heterostructure with the close inset graph of the higher frequencies

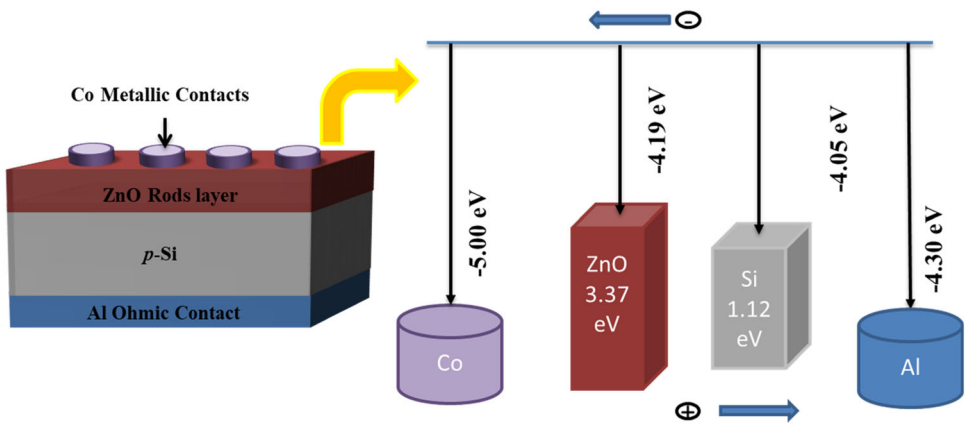

Fig. 1 The schematic (left) and band (right) diagrams of the Co/ZnO-Rods/*p*-Si heterostructures

metal-semiconductor device. However, the peaks were seen in the depletion region due to a low or negligible series resistance effect [28]. The measured capacitance values of these kinds of devices normally change both frequency and bias voltage due to forming of Schottky barrier between metal and semiconductor, series resistance, the impurity level, and the interface states. Whereas the total capacitance value is determined by the only bias-dependent depletion capacitance at lower frequencies, it is controlled by depletion capacitance as well as frequency-dependent bulk resistance at higher frequencies [29]. These results caused the bias-independent capacitance values at higher frequencies according to Fig. 3.

Conductance–voltage (G–V) plots of the Co/ZnO-Rods/p-Si heterostructure are shown in Fig. 4 depending on the increasing frequencies from 10 kHz to 1 MHz. The G–V plots revealed the accumulation, inversion, and depletion regions. The conductance values slowly decreased from the accumulation region to the depletion region. However, the conductance values remained stable in the inversion region for voltage changes. In the case of frequency changes, they exhibited increasing profile with increasing frequency towards 500 kHz and then decreased up to 1 MHz frequency. This kind of behavior can be attributed to reordering and restructuring of the interface states by changing frequency [30].

Interface states and resistance (R_i) are critical parameters to affect the behaviors of metal-semiconductor heterostructures. Nicollian and Brews technique is usually used to determine the resistance profile of the heterostructure. The R_i is expressed by the following equation [31]:

$$R_i = \frac{G_{ma}}{G_{ma}^2 + (\omega C_{ma})^2} \quad (1)$$

where G_{ma} is measured conductance and C_{ma} is measured capacitance, respectively. The ω shows radial frequency.

Figure 5 indicates the R_i versus voltage plot of the Co/ZnO-Rods/p-Si heterostructure based on the frequency changes. The R_i values suddenly increased toward reverse biases due to the shunt resistance effect of the Co/ZnO-Rods/p-Si heterostructure [6]. However, the resistance values exhibited decreasing profile with increasing frequency due to that the ac signals could not be followed by interface states or they were not effective at higher frequencies [32].

Figure 6 shows the C^{-2}–V plots of the Co/ZnO-Rods/p-Si heterostructure depending on the changing frequency. The C^{-2}–V plots have exhibited that the increasing y-intercept values increase with increasing frequency. The slope and extrapolated x-axis intercept of the C^{-2}–V plots can provide to determine barrier height (Φ_b), doping concentration of the acceptor atoms (N_a), and fermi level (E_F) for the Co/ZnO-Rods/p-Si heterostructure. The Φ_b can be calculated by the following equation [33]:

$$\Phi_b = (V_d + E_F) - \Delta\Phi \quad (2)$$

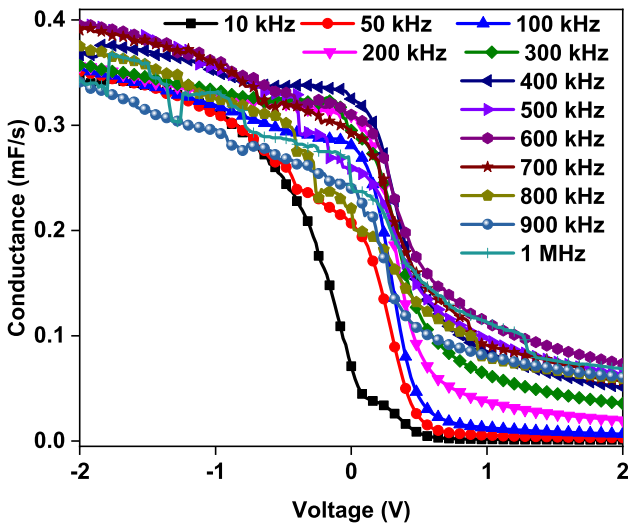

Fig. 4 G–V characteristics of the Co/ZnO-Rods/p-Si heterostructure

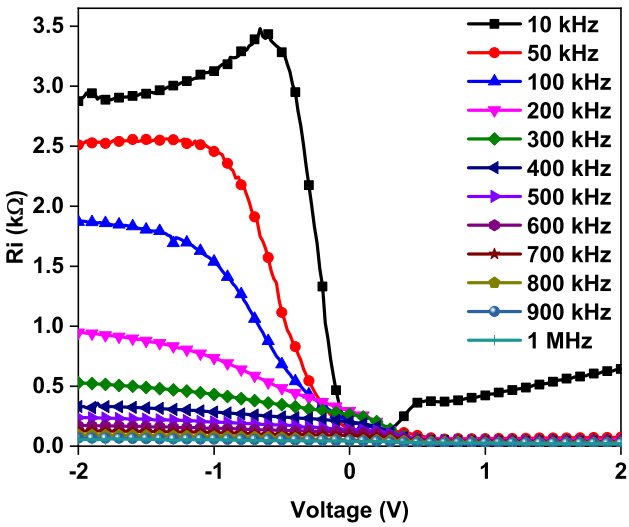

Fig. 5 R_i–V characteristics of the Co/ZnO-Rods/p-Si heterostructure

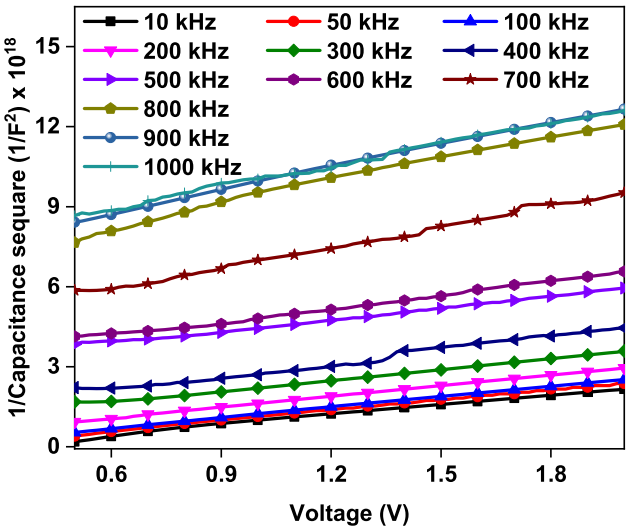

Fig. 6 C^{-2}–V characteristics of the Co/ZnO-Rods/p-Si heterostructure

where $\Delta\Phi$ and V_d show barrier lowering of image force and diffusion potential, respectively. The V_d is the diffusion potential and calculated by $V_d = V_i + kT/q$ formula (V_i shows x-intercept extrapolation). The obtained Φ_b values are tabulated in Table 1 for changing frequency, and their magnitudes usually increased by increasing frequency due to the increasing diffusion potential. The E_F values generally decreased also by decreasing frequency due to increasing slope of the C^{-2}–V plots. The similar results for these parameters can be found in the literature [34, 35].

The other parameters such as length of depletion region (W_d), maximum electric field (E_m), and N_a values also were calculated from the C^{-2}–V plots, and their calculated results are listed in Table 1 for the Co/ZnO-Rods/p-Si heterostructure depending on the frequency. The W_d values increased while the N_a values usually decreased by increasing frequency. However, the E_m values usually increased by increasing frequency until 500 kHz and then slightly decreased.

The Hill–Coleman method can be employed to determine the interface states (N_{ss}) related to the frequency changes. The N_{ss} is addressed by next formula related to the capacitance (C_m) and conductance values (G_m) [36]:

$$N_{ss} = \frac{2}{qA}\frac{(G_m/\omega)_{max}}{((G_m/\omega)_{max}/C_{0x})^2 + (1 - C_m/C_{0x})^2} \quad (3)$$

where A is the device contact area. The C_{0x} is interface capacitance and calculated by the next equation from C_{ma} and G_{ma} values in the case of strong accumulation region:

$$C_{0x} = C_{ma}\left[1 + \frac{G_{ma}^2}{(\omega C_{ma})^2}\right] \quad (4)$$

The N_{ss} values usually decreased by increasing frequency due to that their effectiveness decreased toward higher frequencies [37]. Their values are in good agreement for a kind of metal-semiconductor device [38].

The polarization and conduction mechanisms can be understood by studying various dielectric parameters. Complex dielectric permittivity is given by $\varepsilon^* = \varepsilon' - j\varepsilon''$ formula with real and imaginary

Table 1 Some of electrical parameters for Co/ZnO-Rods/p-Si heterostructure by changing frequency

f (kHz)	N_a (10^{16} cm^{-3})	R_s (Ω)	Φ_b (eV)	E_F (eV)	E_m (10^4 v/cm)	W_d (10^{-5} cm)	N_{ss}(10^{11} eV^{-1} cm^{-2})
10	16.3	487.25	0.21	0.059	8.76	0.38	39.8
50	15.0	213.89	0.18	0.061	7.42	0.36	45.6
100	14.5	226.27	0.13	0.062	5.56	0.30	26.7
200	14.4	192.63	0.26	0.062	9.55	0.46	7.53
300	13.9	158.51	0.63	0.063	15.7	0.76	4.38
400	11.5	121.64	0.70	0.068	15.0	0.88	3.91
500	12.5	149.10	1.90	0.066	26.6	1.41	3.56
600	10.8	108.56	1.72	0.070	23.4	1.44	3.88
700	7.69	112.54	2.23	0.079	22.6	1.94	8.28
800	8.10	83.30	2.43	0.077	24.2	1.98	11.4
900	7.48	65.73	2.62	0.079	24.2	2.14	11.9
1000	6.71	57.44	2.92	0.082	24.2	2.38	9.77

parts. While the real part represents stored energy as well as dipole strength against the applied electric field and called dielectric constant (ε'), the imaginary part is dielectric loss (ε'') and shows absorbed energy due to frictional dampening [39].

The complex permittivity can be addressed as the next equation depending on the capacitance (C) and conductance (G) values:

$$\varepsilon^* = \frac{C}{C_0} - j\frac{G}{\omega C_0} \tag{5}$$

where C_0 represents free capacitor value. If the free capacitor formula ($C_0 = \varepsilon_0 A/d_i$ where A, d_i, and ε_0 are the surface area of the device, interlayer thickness, and vacuum permittivity) is written in the ε' and ε'', following equations can be obtained [20]:

$$\varepsilon' = \frac{C}{C_0} = \frac{Cd_i}{\varepsilon_0 A} \tag{6}$$

$$\varepsilon'' = \frac{G}{\omega C_0} = \frac{Gd_i}{\varepsilon_0 \omega A} \tag{7}$$

Another dielectric parameter is the loss tangent (tan δ) and is given the ratio of the dielectric loss and dielectric constant by the following equation:

$$\tan\delta = \frac{\varepsilon''}{\varepsilon'} = \frac{G}{\omega C} \tag{8}$$

The ε'–V plots of the Co/ZnO-Rods/p-Si heterostructure are indicated in Fig. 7 for the changing frequencies in the range of 10–1000 kHz. The ε' values exhibited peaks at around 0 for lower frequencies, but the peak positions shifted toward forward biases. While the peaks at the dielectric constant depended on the interface states (N_{ss}) as well as series resistance, the decrease at the dielectric constant by increasing frequency can be ascribed to that higher frequencies cannot be followed by N_{ss} [40, 41]. These kinds of changes with voltage and frequency at the ε' values might depend on the Maxwell–Wagner-type polarization owing to charge accumulation at the grain boundaries [42]. The results are in good harmony with the dielectric constant of ZnO-based devices [43, 44].

The dielectric loss (ε'') when plotted against to voltage changes of the Co/ZnO-Rods/p-Si heterostructure is exhibited in Fig. 8 for various frequencies. The ε'' values displayed inversion, depletion, and accumulation regions, and their values

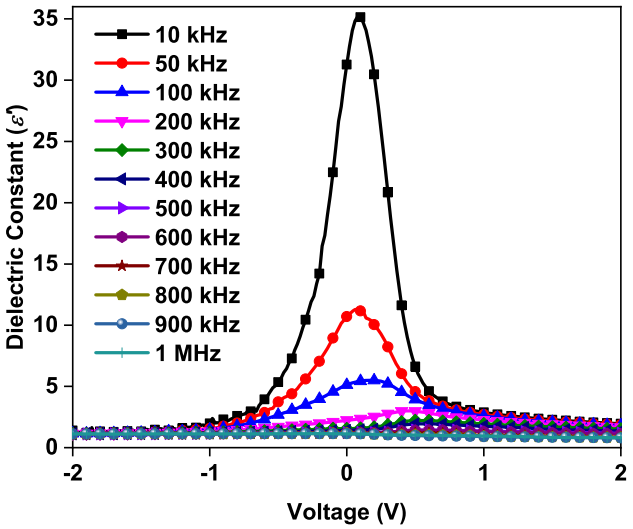

Fig. 7 The ε'–V plots of the Co/ZnO-Rods/p-Si heterostructure depending on the frequency changes

remained stable in the inversion region with changing frequency and voltage. However, the ε'' values exhibited decreasing profile with increasing frequency in the case of accumulation region. This kind of behavior at the ε'' values can be ascribed to the interface states and series resistance effects [45].

Figure 9 and its inset close look graph show tan δ versus voltage plots of the Au/ZnO/p-Si heterostructure related to the changing frequency. The tan δ values almost did not change in the inversion region depending on the voltage and frequency, but they decreased with increasing

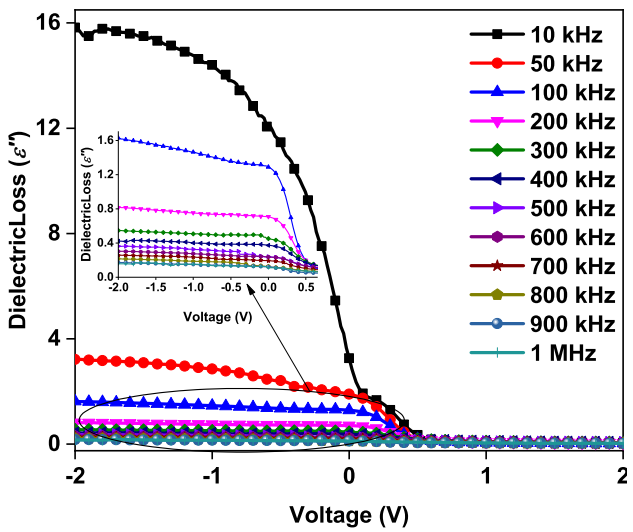

Fig. 8 The ε''–V graphs of the Co/ZnO-Rods/p-Si heterostructure for frequency changes

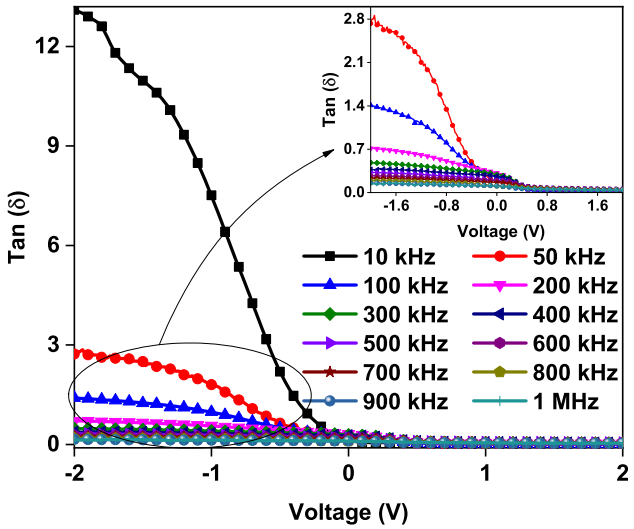

Fig. 9 The tan δ–V curves of the Co/ZnO-Rods/p-Si heterostructure for changing frequency

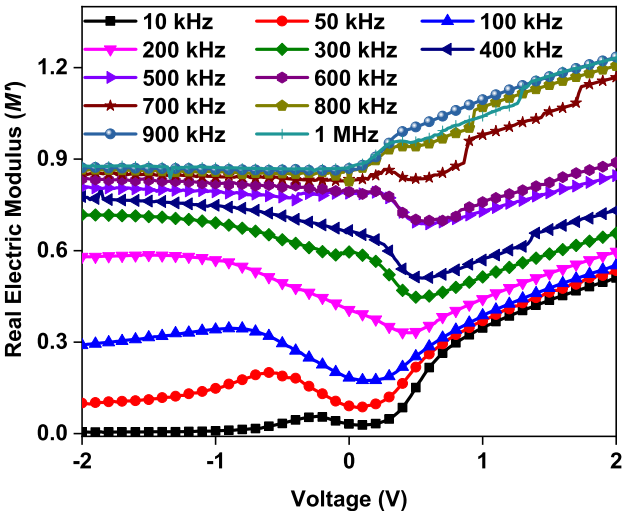

Fig. 10 The M'–V plots of the Co/ZnO-Rods/p-Si heterostructure for frequency changes

frequency in the accumulation region. This behavior also can be attributed to presence of the interface states and series resistance in the heterostructure [46].

The complex electric modulus (M^*) is another important parameter to understand the relaxation process and can be obtained by the formalism of $\varepsilon^*=1/M^*$ by reciprocal of the complex electric modulus [47]. The M^* has a real and imaginary part and is given by $M^*=M^{'}+jM''$. The $M^{'}$ and M'' values can be written as the next formula related to the $\varepsilon^{'}$ and $\varepsilon^{''}$ values:

$$M^* = \frac{1}{\varepsilon^*} = \frac{\varepsilon'}{\varepsilon'^2+\varepsilon''^2} + j\frac{\varepsilon''}{\varepsilon'^2+\varepsilon''^2} = M^{'} + jM'' \tag{9}$$

M'–V plots of the Co/ZnO-Rods/p-Si heterostructure are indicated in Fig. 10 for the frequency range of 10 kHz and 1 MHz. The M' values generally enhanced by enhancing frequency in accumulation, depletion, and inversion regions. However, they exhibited different profiles for changing frequency. The altering at the M' values due to voltage change and frequency can be attributed to the relaxation of the polarization [48].

The M''–V plots of the Co/ZnO-Rods/p-Si heterostructure are displayed in Fig. 11 related to the frequency changes. The M'' values increased with enhancing frequency for the first three frequencies of 10 kHz, 50 kHz, and 100 kHz and then diminished periodically with enhancing frequency in the depletion and accumulation regions. In the case of the inversion region, the slight increases are seen at the

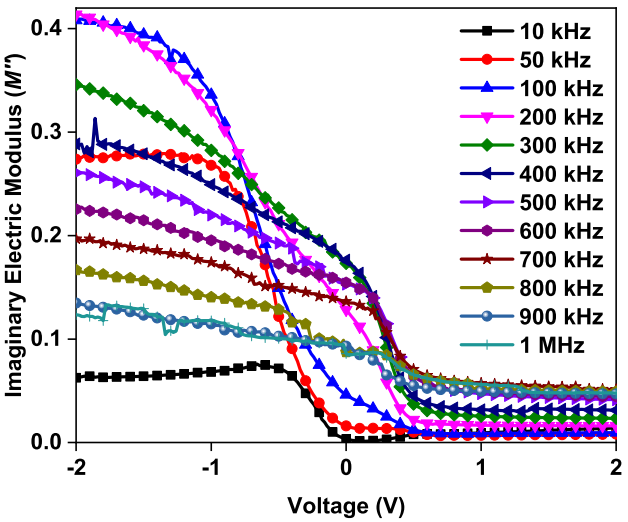

Fig. 11 The M''–V plots of the Co/ZnO-Rods/p-Si heterostructure related to the changing frequency

M'' values with increasing frequency. This alteration at the M'' values with changing frequency can depend on relaxation time of interface states [6, 49].

The ac electric conductivity (σ) can be given by the following equation depending on the ε'' values:

$$\sigma = \left(\frac{d}{A}\right)\omega C\tan\delta = \varepsilon^{''}\omega\varepsilon_0 \tag{10}$$

Figure 12 shows the σ–V plots of the Co/ZnO-Rods/p-Si heterostructure for the frequencies between 10 kHz and 1 MHz. The σ values diminished from accumulation to depletion region and stayed without change in the inversion region for a

given frequency. In the case of changing frequency, the σ values generally increased up to 600 kHz frequency and then diminished except 1 MHz frequency. These kinds of fluctuation at the σ values might depend on the reordering and restructuring of the interface states with changing frequency. The increase of the σ values caused by eddy current due to decreasing series resistance as well as hoping of charge carrier from the traps [37, 48, 50]. The reduction at the σ values with increasing frequency after 600 kHz may be ascribed to the interface states that cannot be able to have enough time to follow higher frequencies.

4 Conclusion

ZnO-Rods film was obtained by spray pyrolysis technique on the *p*-Si substrate to fabricate Co/ZnO-Rods/*p*-Si heterostructure. SEM image of ZnO-Rods confirmed the smooth and homogenous surface as well as rod-like structures. The *C*–*V* and *G*–*V* measurements were employed for the Co/ZnO-Rods/*p*-Si heterostructure to characterize the electrical and dielectric properties depending on changing frequency. The *C*–*V* characteristics indicated that the Co/ZnO-Rods/*p*-Si heterostructure showed peaks and the position of the peaks shifted due to interface states. The *G*–*V* characteristics clearly showed accumulation, depletion, and inversion region of the Co/ZnO-Rods/*p*-Si heterostructure. The C^{-2}–*V* plot was used to determine various electrical parameters and examined paper related to the changing frequency. The Co/ZnO-Rods/*p*-Si heterostructure exhibited higher ε' values, but their values decreased by enhancing frequency. Both the ε'' and tan δ values displayed decreasing profile with enhancing frequency in the accumulation region. While the M' values increased with increasing frequency, the M'' values had an increasing profile up to 200 kHz and the decreasing profiles up to 1 MHz frequency in the accumulation region. The σ values have both increasing and decreasing profile due to restructuring and reordering of the interface states related to frequency changes. The results highlight that the Co/ZnO-Rods/*p*-Si heterostructure can be employed for switching applications.

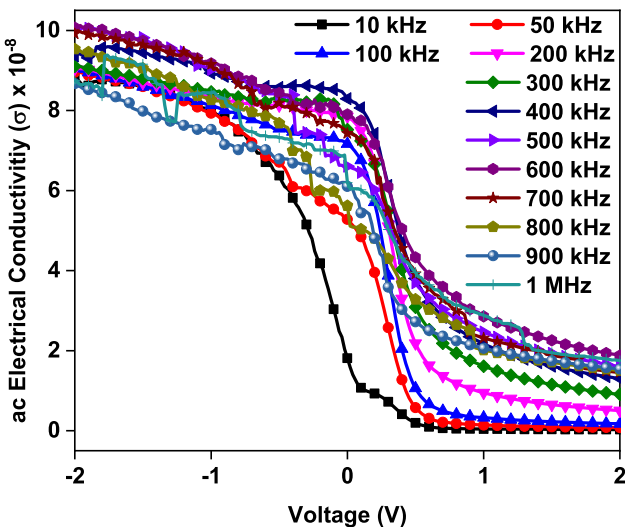

Fig. 12 The σ–*V* plots of the Co/ZnO-Rods/*p*-Si heterostructure depending on various frequencies

Acknowledgements

The authors thank Fatma Yildirim and Zeynep Orhan for their technical assistance with this study.

Author contributions

All authors have equal contribution to the study.

Data availability

The raw data are available at the corresponding author and can be presented for reasonable requests.

Declarations

Conflict of interest The authors declare that they have no conflict of interest.

References

1. X. Yu, T.J. Marks, A. Facchetti, Metal oxides for optoelectronic applications. Nat. Mater. **15**, 383–396 (2016). https://doi.org/10.1038/nmat4599
2. Z. Yan, Y. Wang, D. Zeng, D.B. Chrisey, M. Liu, Multifunctionalization of Nanostructured Metal Oxides. J. Nanomater. (2015). https://doi.org/10.1155/2015/102976
3. G. Zhang, X. Xiao, B. Li, P. Gu, H. Xue, H. Pang, Transition metal oxides with one-dimensional/one-dimensional-analogue nanostructures for advanced supercapacitors. J. Mater.

Chem. A **5**, 8155–8186 (2017). https://doi.org/10.1039/c7ta02454a
4. N. Tripathy, D.H. Kim, Metal oxide modified ZnO nanomaterials for biosensor applications. Nano Converg. **5**, 1–10 (2018). https://doi.org/10.1186/s40580-018-0159-9
5. M. Yilmaz, Investigation of characteristics of ZnO: Ga nanocrystalline thin films with varying dopant content. Mater. Sci. Semicond. Process. **40**, 99–106 (2015). https://doi.org/10.1016/j.mssp.2015.06.031
6. I. Orak, A. Kocyigit, S. Alindal, Electrical and dielectric characterization of Au/ZnO/n-Si device depending frequency and voltage. Chin. Phys. B **26**, 028102-028102–028107 (2017). https://doi.org/10.1088/1674-1056/26/2/028102
7. B. Ezhilmaran, A. Patra, S. Benny, M.R. Sreelakshmi, V.V. Akshay, S.V. Bhat, C.S. Rout, Recent developments in the photodetector applications of Schottky diodes based on 2D materials. J. Mater. Chem. C **9**, 6122–6150 (2021). https://doi.org/10.1039/d1tc00949d
8. M. Das, A. Kumar, B. Mandal, M.T. Htay, S. Mukherjee, Impact of Schottky junctions in the transformation of switching modes in amorphous Y2O3-based memristive system. J. Phys. D **51**, 315102 (2018). https://doi.org/10.1088/1361-6463/aacf14
9. J. Yang, C. Fares, F. Ren, Y.-T. Chen, Y.-T. Liao, C.-W. Chang, J. Lin, M. Tadjer, D.J. Smith, S.J. Pearton, A. Kuramata, Switching behavior and forward bias degradation of 700V, 02A, β-Ga2O3 vertical geometry rectifiers. ECS J. Solid State Sci. Technol. **8**, Q3028 (2019). https://doi.org/10.1149/2.0061907JSS
10. Y. Wang, S. Yang, A. Ballesio, M. Parmeggiani, A. Verna, M. Cocuzza, C.F. Pirri, S.L. Marasso, The fabrication of Schottky photodiode by monolayer graphene direct-transfer-on-silicon. J. Appl. Phys. (2020). https://doi.org/10.1063/5.0004242
11. H. Guan, C. Jiang, Study on the Physical and Leakage Current Characteristics of an Optimized High-k/InAlAs MOS Capacitor with a HfO2–Al2O3 Laminated Dielectric. Coatings **8**, 417 (2018). https://doi.org/10.3390/COATINGS8120417
12. R.T. Tung, Formation of an electric dipole at metal-semiconductor interfaces. Phys. Rev. B **64**, 205310 (2001). https://doi.org/10.1103/PhysRevB.64.205310
13. Ç. Bilkan, S. Zeyrek, S.E. San, Ş Altındal, A compare of electrical characteristics in Al/p-Si (MS) and Al/C20H12/p-Si (MPS) type diodes using current–voltage (I–V) and capacitance–voltage (C–V) measurements. Mater. Sci. Semicond. Process. **32**, 137–144 (2015). https://doi.org/10.1016/J.MSSP.2014.12.071
14. A. Kocyigit, İ Karteri, I. Orak, S. Uruş, M. Çaylar, The structural and electrical characterization of Al/GO-SiO2/p-Si photodiode. Phys. E Low-Dimensional Syst. Nanostruct. **103**, 452–458 (2018). https://doi.org/10.1016/j.physe.2018.06.006
15. A. Kocyigit, I. Orak, The electrical characterization effect of insulator layer between semiconductor and metal. J. Inst. Sci. Technol. **6**, 57–57 (2016). https://doi.org/10.21597/jist.2016321840
16. S.O. Tan, O. Çiçek, Ç.G. Türk, Ş Altındal, Dielectric properties, electric modulus and conductivity profiles of Al/Al2O3/p-Si type MOS capacitor in large frequency and bias interval. Eng. Sci. Technol. Int. J. (2021). https://doi.org/10.1016/j.jestch.2021.05.021
17. A. Barkhordari, S. Ozcelik, Ş Altindal, G. Pirgholi-Givi, H. Mashayekhi, Y. Azizian-Kalandaragh, The effect of PVP: BaTiO3interlayer on the conduction mechanism and electrical properties at MPS structures. Phys. Scr. **96**, 085805 (2021). https://doi.org/10.1088/1402-4896/abeba8
18. S. Demirezen, E.E. Tanrıkulu, Altındal, The study on negative dielectric properties of Al/PVA (Zn-doped)/p-Si (MPS) capacitors. Indian J. Phys. **93**, 739–747 (2019). https://doi.org/10.1007/s12648-018-1355-5
19. Y. Badali, Ş Altındal, İ Uslu, Dielectric properties, electrical modulus and current transport mechanisms of Au/ZnO/n-Si structures. Prog. Nat. Sci. Mater. Int. **28**, 325–331 (2018). https://doi.org/10.1016/j.pnsc.2018.05.003
20. S. Demirezen, Frequency- and voltage-dependent dielectric properties and electrical conductivity of Au/PVA (Bi-doped)/n-Si Schottky barrier diodes at room temperature. Appl. Phys. A **112**, 827–833 (2013). https://doi.org/10.1007/s00339-013-7605-7
21. M. Yildirim, A. Kocyigit, A systematic study on the dielectric relaxation, electric modulus and electrical conductivity of Al/Cu:TiO2n-Si (MOS) structures/capacitors. Surf. Rev. Lett. **27**, 1950217 (2020). https://doi.org/10.1142/S0218625X19502172
22. M. Soosen Samuel, J. Koshy, A. Chandran, K.C. George, Dielectric behavior and transport properties of ZnO nanorods. Phys. B. **406**, 3023–3029 (2011). https://doi.org/10.1016/j.physb.2011.04.070
23. R. Saravanan, T. Prakash, V.K. Gupta, A. Stephen, Tailoring the electrical and dielectric properties of ZnO nanorods by substitution. J. Mol. Liq. **193**, 160–165 (2014). https://doi.org/10.1016/j.molliq.2013.12.029
24. A. Buyukbas-Ulusan, I. Taşçıoğlu, A. Tataroğlu, F. Yakuphanoğlu, S. Altındal, A comparative study on the electrical and dielectric properties of Al/Cd-doped ZnO/p-Si structures. J. Mater. Sci. Mater. Electron. **30**, 12122–12129 (2019). https://doi.org/10.1007/s10854-019-01570-z
25. E. Kärber, T. Raadik, T. Dedova, J. Krustok, A. Mere, V. Mikli, M. Krunks, Photoluminescence of spray pyrolysis

deposited ZnO nanorods. Nanoscale Res. Lett. **6**, 1–7 (2011). https://doi.org/10.1186/1556-276X-6-359

26. S.C. Singh, Zinc oxide nanostructures; synthesis, characterizations and device applications. J. Nanoeng. Nanomanufact. **3**, 283–310 (2013). https://doi.org/10.1166/jnan.2013.1147
27. S.E. Meftah, M. Benhaliliba, M. Kaleli, C.E. Benouis, C.A. Yavru, A.B. Bayram, Optical and electrical characterization of thin film MSP heterojunction based on organic material Al/p-Si/P3HT/Ag. Phys. B **593**, 412238 (2020). https://doi.org/10.1016/j.physb.2020.412238
28. Y.D. Wang, J. Chen, Modeling capacitance-voltage characteristic of TiW/p-InP Schottky barrier diode. Chin Phys. B **27**, 097203 (2018). https://doi.org/10.1088/1674-1056/27/9/097203
29. I. Hussain, M.Y. Soomro, N. Bano, O. Nur, M. Willander, Interface trap characterization and electrical properties of Au-ZnO nanorod Schottky diodes by conductance and capacitance methods. J. Appl. Phys. **112**, 064506 (2012). https://doi.org/10.1063/1.4752402
30. A. Tataroğlu, Ş Altindal, M.M. Bülbül, Temperature and frequency dependent electrical and dielectric properties of Al/SiO2/p-Si (MOS) structure. Microelectron. Eng. **81**, 140–149 (2005). https://doi.org/10.1016/j.mee.2005.04.008
31. E.H. Nicollian, J.R. Brews, *MOS (metal oxide semiconductor) physics and technology* (Wiley-Interscience, New York, 2003)
32. A. Boutelala, F. Bourfa, M. Mahtali, Effect of light on electrical and photoelectrical characteristics of Al/TiO2/p-Si Schottky diode. J. Mater. Sci. Mater. Electron. **31**, 11379–11389 (2020). https://doi.org/10.1007/s10854-020-03687-y
33. İ Orak, A. Koçyiğit, The thickness effect of insulator layer between the semiconductor and metal contact on C–V characteristics of Al/Si3N4/p-Si device, Pamukkale Univ. J Eng. Sci. **23**, 536–542 (2017). https://doi.org/10.5505/pajes.2016.23911
34. E.E. Tanrıkulu, S. Demirezen, Ş Altındal, İ Uslu, On the anomalous peak and negative capacitance in the capacitance–voltage (C–V) plots of Al/(%7 Zn-PVA)/p-Si (MPS) structure. J. Mater. Sci. Mater. Electron. **29**, 2890–2898 (2018). https://doi.org/10.1007/s10854-017-8219-1
35. S. Demirezen, İ Orak, Y. Azizian-Kalandaragh, Ş Altındal, Series resistance and interface states effects on the C-V and G/w–V characteristics in Au/(Co3O4-doped PVA)/n-Si structures at room temperature. J. Mater. Sci. Mater. Electron. **28**, 12967–12976 (2017). https://doi.org/10.1007/s10854-017-7128-7
36. W.A. Hill, C.C. Coleman, A single-frequency approximation for interface-state density determination. Solid. State. Electron. **23**, 987–993 (1980). https://doi.org/10.1016/0038-1101(80)90064-7
37. S. Nezhadesm-Kohardafchahi, S. Farjami-Shayesteh, Y. Badali, Ş Altındal, M.A. Jamshidi-Ghozlu, Y. Azizian-Kalandaragh, Formation of ZnO nanopowders by the simple ultrasound-assisted method: Exploring the dielectric and electric properties of the Au/(ZnO-PVA)/n-Si structure. Mater. Sci. Semicond. Process. **86**, 173–180 (2018). https://doi.org/10.1016/j.mssp.2018.06.030
38. N.A. Al-Ahmadi, Metal oxide semiconductor-based Schottky diodes: a review of recent advances. Mater. Res. Express. **7**, 032001 (2020). https://doi.org/10.1088/2053-1591/ab7a60
39. Ş Karataş, Studies on electrical and the dielectric properties in MS structures. J. Non. Cryst. Solids. **354**, 3606–3611 (2008). https://doi.org/10.1016/J.JNONCRYSOL.2008.03.028
40. S. Alptekin, A. Tataroğlu, Ş Altındal, Dielectric, modulus and conductivity studies of Au/PVP/n-Si (MPS) structure in the wide range of frequency and voltage at room temperature. J. Mater. Sci. Mater. Electron. **30**, 6853–6859 (2019). https://doi.org/10.1007/s10854-019-00998-7
41. A.M. Akbaş, A. Tataroğlu, Ş Altındal, Y. Azizian-Kalandaragh, Frequency dependence of the dielectric properties of Au/(NG:PVP)/n-Si structures. J. Mater. Sci. Mater. Electron. **32**, 7657–7670 (2021). https://doi.org/10.1007/s10854-021-05482-9
42. D.E. Yıldız, I. Dökme, Frequency and gate voltage effects on the dielectric properties and electrical conductivity of Al/SiO2/p-Si metal-insulator-semiconductor Schottky diodes. J. Appl. Phys. **110**, 014507 (2011). https://doi.org/10.1063/1.3602090
43. R. Aepuru, S. Kankash, H.S. Panda, Schottky barrier tuning in semiconducting ZnO and BaTiO3 hybrid heterostructures shows dielectric and electrical anisotropy. RSC Adv. **6**, 32272–32285 (2016). https://doi.org/10.1039/c6ra00841k
44. A. Kocyigit, I. Orak, A. Turut, Temperature dependent dielectric properties of Au/ZnO/n-Si heterojuntion. Mater. Res. Express. (2018). https://doi.org/10.1088/2053-1591/aab2e3
45. T. Ataseven, A. Tataroglu, T. Memmedli, S. Özçelik, Influence of frequency on electrical and dielectric properties of Au/Si 3N 4/n-Si (MIS) structures. J. Optoelectron. Adv. Mater. **14**, 640–645 (2012)
46. S. Türkay, A. Tataroğlu, Complex dielectric permittivity, electric modulus and electrical conductivity analysis of Au/Si3N4/p-GaAs (MOS) capacitor. J. Mater. Sci. Mater. Electron. **32**, 11418–11425 (2021). https://doi.org/10.1007/s10854-021-05349-z
47. H.G. Çetinkaya, S. Alialy, Ş Altındal, A. Kaya, İ Uslu, Investigation of negative dielectric constant in Au/1% graphene (GP) doped-Ca19Pr01Co4Ox/n-Si structures at

forward biases using impedance spectroscopy analysis. J. Mater. Sci. Mater. Electron. **26**, 3186–3195 (2015). https://doi.org/10.1007/s10854-015-2816-7

48. Ç. Bilkan, Y. Azizian-Kalandaragh, Ş Altındal, R. Shokrani-Havigh, Frequency and voltage dependence dielectric properties, ac electrical conductivity and electric modulus profiles in Al/Co3O4-PVA/p-Si structures. Phys. B **500**, 154–160 (2016). https://doi.org/10.1016/j.physb.2016.08.001
49. A. Kaya, S. Alialy, S. Demirezen, M. Balbaşı, S.A. Yerişkin, A. Aytimur, The investigation of dielectric properties and ac conductivity of Au/GO-doped PrBaCoO nanoceramic/n-Si capacitors using impedance spectroscopy method. Ceram. Int. **42**, 3322–3329 (2016). https://doi.org/10.1016/j.ceramint.2015.10.126
50. Ö. Sevgili, İ Taşçoığlu, S. Boughdachi, Y. Azizian-Kalandaragh, Ş Altındal, Examination of dielectric response of Au/HgS-PVA/n-Si (MPS)structure by impedance spectroscopy method. Phys. B **566**, 125–135 (2019). https://doi.org/10.1016/j.physb.2019.04.029